The Future of Advanced Propellantless Propulsion

Dennis Lee[1]
Vortex Space Systems, LLC, Germantown, Maryland, 20876, USA

Vortex Space Systems, LLC (VSS) is uniquely qualified to develop the future of CAM drive Minimum Viable Product (MVP) propellantless propulsion, which has significant propulsive and business economic advantages. MVP development is supported by a Montgomery County (Maryland) Technology Innovation Fund grant is called StarVoyager, starting in August 2025. StarVoyager propellantless MVP is designed to meet the small satellite market with operations between Very Low Earth Orbit (VLEO) and LEO altitudes. Prior, National Science Foundation (NSF) provided a Small Business Technology Transfer (STTR) Phase I grant funding for Active Debris Removal (ADR), called Hyper Transfer Vehicle (HTV). The NSF study was awarded to VSS in April 2023. The Conservation of Angular Momentum (CAM) methods were used for analyzing HTV and MVP performance test data.

Introduction

CAM drive propellantless propulsion offers methods to reduce propulsion system launch costs, flexible orbit profiles, and disposal. CAM drive physics uses circulating working fluid to define propellantless propulsion and solve the rocket's inherent limitation, which is the propulsive fuel. Instead of expelling propellant, CAM drive rotates a working fluid reaction mass with Electric Ducted Fan (EDF) motors inside a toroidal cavity. This action generates a measurable reaction force and provides thrust that is perpendicular to the symmetric torus tube, Fig. 1. CAM drive is consistent with NASA's space drive definition [1], by defining CAM as the conservation method and transferring momentum via working fluid. CAM drive propellantless technology provides reusable and high cadence solutions for LEO missions with clean Solar Electric Power (SEP).

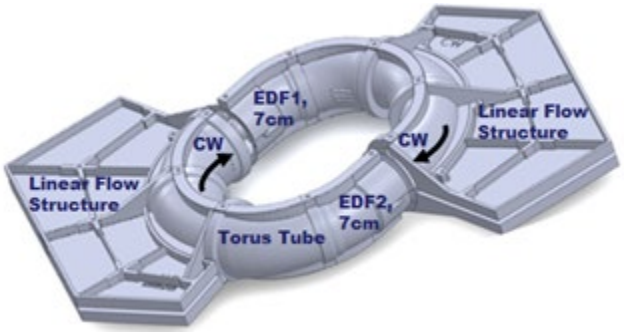

Figure 1: Versatile and Modular CAM drive uses Air as Working Fluid

The MVP CAM drive outperforms all Hall and ion orbit transfer thrusters in Table 1. Hall and ion thrusters have not crossed the 1 Newton (N) thruster force barrier in 25 years of research and development. The thrust performance is well above 1N thruster force limit, Table 1, for ADR servicing missions.

Table 1: SEP Thruster Comparisons

Thruster	Company	Performance (N)	Power (kWatts)	Application
AEPS	Aerojet-Rocketdyne	0.590	12.5	NASA, Lunar Gateway
BHT-6000	Busek Hall Thruster	0.2 – 0.329	6.0	NASA, Lunar Gateway
HTV, NSF Phase I STTR	VSS	5.0 (peak)	8.3 (average)	VSS NSF Phase I ADR Study
IHET-300	Rafael (Israel)	0.014	0.30	ISA/CNES, VENuS mission
RIT-10	Safran (France)	0.015	0.435	Clarity-1, US Earth Observation
Average CAM drive MVP	VSS	0.80 (measured)	0.46 (measured)	LEO/VLEO, Fig. 14
Peak CAM drive	VSS	2.5 (estimated)	2.0 (estimated)	LEO/VLEO, Section 7

[1] VSS, LLC Owner/CEO, and AIAA Member.

Acknowledge National Science Foundation (NSF) STTR Phase I Grant #2233424
Montgomery County (Maryland) Technology Innovation Fund Grant

MVP CAM drive increases performance over commercial Hall thrusters. In Table 1, power requirements are identified for Hall and propellantless propulsion. An average CAM drive thrust performance of 800mN is clearly above NASA's AEPS at 590mN. It is CAM drive's 460W of power versus AEPS 12.5kW that establishes the economic advantage. Satellite solar array power systems cost about $1.5M per kilowatt. In this comparison, CAM drive savings is $18M just from the power system.

Discussion

1. Background

NSF Phase I HTV used air as a working fluid reaction mass with EDFs moving air inside a toroidal cavity structure, Fig. 2. CAM drive rotates working fluid at high angular rates inside the torus tube while mounted inside a pressurized enclosure separate from the vacuum of space. The clockwise (CW) and counterclockwise (CCW) circulation working fluid direction is the difference between identical structures. Both top and bottom torus tubes have tangential slot opening that breaks the torque free symmetry allowing working fluid flow into the linear flow cavity. Fig. 2 shows EDFs circulating the working fluid inside two separate and identical torus tube cavities at high rates of 10Hz to 20Hz.

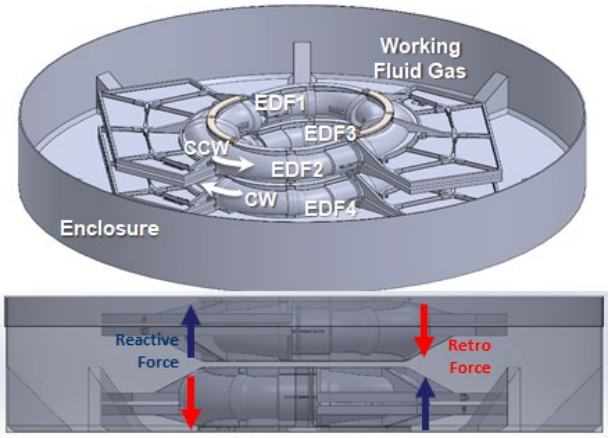

Figure 2: Angular Momentum Couples with EDF1/3 Reactive Force and EDF2/4 for Retroactive Force

NSF Phase I showed the effects of symmetry breaking by generating angular momentum couples between EDF1/3 (blue) reactive force and EDF2/4 (red) retroactive force, Fig. 2. Controlling reaction forces and couples with CW and CCW working fluid polarity were important discoveries in NSF Phase I test data. This discovery lead to the concept of operation by using EDF1/3 together for motion in the reactive direction and EDF2/4 in the opposite direction. The NSF Phase I testing demonstrated HTV force throttling capability.

In 1927, W.R. Dean studied fluid flows in a 90º elbow in dynamic equilibrium [2]. Dean flows are examples of torque free fluid motion with two counterrotating poloidal flows in symmetric equilibrium. In nature, counterrotating Dean flows are the distribution of angular momentum vectors with equal and opposite torques that conserve the fluid's angular momentum and rotational energy, Fig. 3.

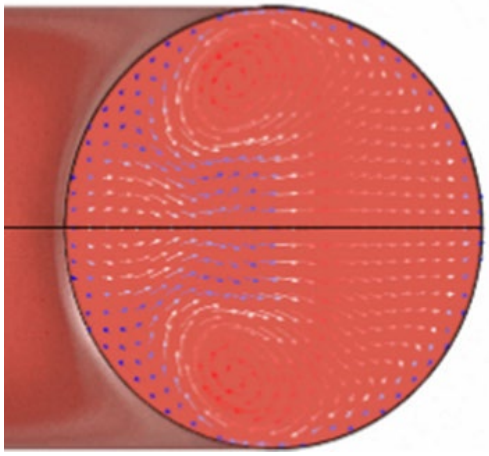

Figure 3: Dean flows in 90º Elbow Demonstrate LBM Stable Circular (Poloidal) Flows

Navier-Stokes (NS) Computational Fluid Dynamics (CFD) studies demonstrate symmetric Dean flow analytical results for 90º elbows, [3]. Also, the Lattice Boltzmann Method (LBM) CFD analysis demonstrates Dean flows, Fig. 3. The LBM numerical schemes use microscopic physics, and can recover accurate solutions of the macroscopic, like the Navier-Stokes equations.

In nature and technology, there are examples of torque free or counter-rotating symmetric flows including Dean flows in Fig. 3, spiral vortex sheets, wing tip vortices, and counter-rotating eddies of water observed by Leonardo DaVinci, who believed that water was the "vehicle of nature." Sustained asymmetric rotating fluid flows are observed in the Magnus effect and Kutta airfoil vortex sheet, which generate inertial lift forces. These examples lead to the *CAM Hypothesis*: If counter-rotating hydro/aerodynamic vortexes satisfy CAM principles, such as Dean flows, then an asymmetric CAM drive circulating flows must

generate a CAM compliant force with measurable reaction forces resulting from Euler's inertial fluid system moments.

The Montgomery County (Maryland) Technology Innovation Fund grant is testing of three prototypes, including a prototype for Helmholtz 1st theorem in hydrodynamics with University of Maryland intern engineering students. Helmholtz theorem stated that vortex strength, defined as fluid circulation times the cross-section area, $\boldsymbol{\omega} \cdot A$, is constant along a fluid filament for inviscid flows. Helmholtz theorem means a vortex filament circulation can increase by changing the circulation cross-section from a larger to smaller area, expanded upon in Section 7. This improvement is achieved with an increase in EDF inlet area of 12cm diameter and reduced in torus tube cavity area with 7cm cross-section, Fig. 4.

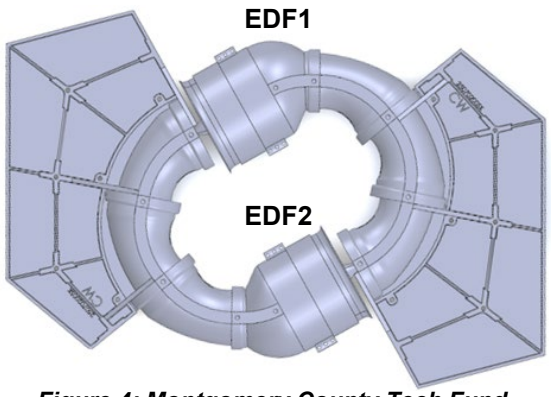

Figure 4: Montgomery County Tech Fund, Helmholtz Test MVP Prototype

2. Rotating System of Particles, Fixed Frame

The CAM drive innovation employs working fluid angular momentum and energy transfer using CAM analysis for a system of particles. CAM is preserved by $d(\boldsymbol{\omega} \cdot \mathbf{H})/dt = d\boldsymbol{\omega} \cdot \mathbf{H} + \boldsymbol{\omega} \cdot d\mathbf{H} = d(2T_{rot})$, where $dT_{rot} = 0$ for energy conservation, $d\boldsymbol{\omega} \cdot \mathbf{H} = 0$ for torque free motion[4] and $d\mathbf{H}$ is the applied torque term. In a system of particles, momentum and energy transfers are only allowed through changes in $\mathbf{H}$ and $\boldsymbol{\omega}$. With symmetric and torque free motion, $d(\boldsymbol{\omega})/dt = \mathbf{0}$ or constant $\mathbf{H}$, there are no momentum and energy transfers. Conserved angular momentum is $\mathbf{H} = I \cdot \boldsymbol{\omega}$. $\mathbf{H}$ is defined by the angular rate vector, $\boldsymbol{\omega} = \mathbf{V}/R$ and inertial working fluid mass (M) distribution with minor moment of inertia (MOI), $I_x = \Sigma_x(y^2+z^2)\, dM$, and major MOI, $I_z = \Sigma_z(x^2+y^2)\, dM$. The generalized, physical model is shown in Fig. 5 as a rotating system block diagram.

The three-axis graphic, Fig. 5, provides for Y-axis continuity with state variables (P,ρ,T) and velocity (V). One-dimensional state properties (P,ρ,T) are given along the Y-axis streamline for incompressible flow with dp/dρ equal to an isothermal constant, a^2, Fig 5. The Y-axis defines I_y transverse MOI, which is evident inside the linear flow assembly cavity and defines the separatrix line.

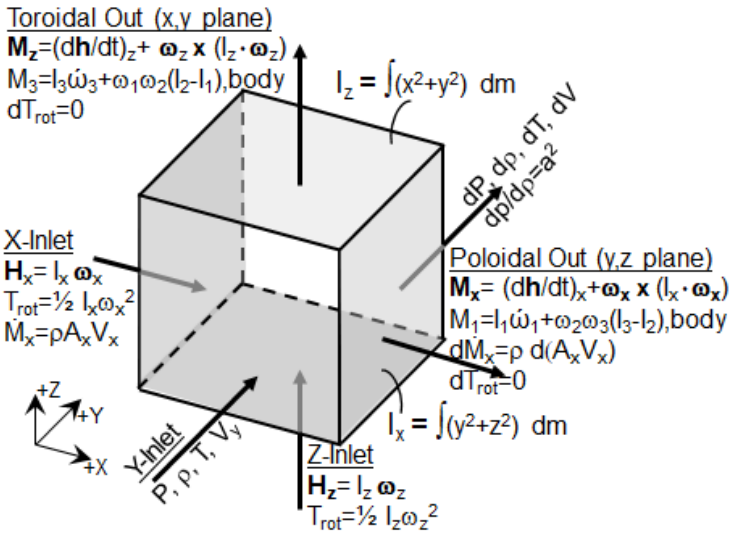

Figure 5: Physical 3D Block Diagram for Rotational System of Particles

Separatrix lines are important boundary conditions for asymmetric dynamic flows, which results from the linear flow structure cavity. As working fluid flow leaves the torus tube through the tangential slot, linear flow is characterized as self-organizing streamlines, tangent to the toroidal working fluid flow. Inside the linear flow cavity, working fluid streamlines are observed and measured, Fig. 10, Section 4.

The CAM flow definition comes from the classic Poinsot geometric solution[4], specifically the oblate solution for nonsymmetric mass distribution, $I_x \neq I_y \neq I_z$. Poinsot's solution constrained both conservation of rotational kinetic energy and the conservation of angular momentum on the motion of angular rate vector,

$\boldsymbol{\omega}(t)$. Poinsot's solution describes torque free angular rate vector $\pm\boldsymbol{\omega}$ as an oblate ellipsoid with a vertex at the center of rotation and its endpoints a circle above and below the plane of symmetry. The ellipsoid represents the full and complete solution set of angular rates ($\boldsymbol{\omega}$'s) that satisfy both conservation for angular momentum and rotational energy[4]. Torque free precession of $\boldsymbol{\omega}(t)$ is the physical analog of Dean flows for equal and symmetric MOIs, $I_x = I_y$, which is defined for symmetric and ideal geometric torus.

Explorer I satellite is a novel example of stable rotation about X-axis moving into the Z-axis with angular momentum transfer through Y-axis separatrix[4]. Explorer I was United States first orbiting spacecraft on a mission to study earth's radiation belts. With stable rotation about the X-axis (minor MOI) and Z-axis (major MOI), the closed polhode curves are traced with $\boldsymbol{\omega}$ fixed in the body frame. Separatrix line defines angular velocity that divides the polhode motion between X-axis and Z-axes. The Explorer I example demonstates the significant difference between solid body rotation and working fluid rotation. For solid bodies, angular momentum can distribute only on one MOI axis at a time. Where circulating working fluid rotation can exist on both the X- and Z-axis at the same time.

To create an inertial force and angular momentum couples, CAM drive leverages Euler moments and manipulates natural CAM invariants from asymmetric solid body rotation. The CAM natural invariant properties are embodied in the models and field equations. These properties include inertial space herpolhode trajectories on the invariable plane[4]. This feature ties the poloidal working fluid to inertial frame dragging described in Helmholtz 2nd theorem of vorticity, expanded upon in Section 7. These physical conservation principles are truth models that support consistent experimentation and repeatable propellantless CAM drive analyses.

3. CAM Drive Working Fluid Analysis

In the CAM Hypothesis, working fluid is circulating and forces are associated with conservation principles. The NSF Phase I linear regression data analysis have positive and negative slopes for CCW and CW working fluid flow, respectively. The Phase I data linear regression analysis, Fig. 6, shows the relevance for separatrix line symmetry breaking in Poinsot geometric CAM solution for CW working fluid, Fig. 7. The analysis of Poinsot's ellipsoid solution in the body frame shows a direct correlation with CAM principles measured in CAM drive fluid flows and forces, Figs. 7 and 8. Specifically, the relationships between observed working fluid flow patterns that trace $\boldsymbol{\omega}$ in poloidal and toroidal flows and the physical position of the red separatrix line.

The separatrix line defines the physical phase-space boundary for the angular velocity vector $\boldsymbol{\omega}$ between blue lines for poloidal (X-MOI) and green lines for toroidal (Z-MOI) flows. An analogy for separatrix line is an inertial wall forming a physical barrier that constrains angular velocity to single side between the X and Z-axis flow. The angular velocity and angular momentum fluid motion can move away from the separatrix line, while converging around the Z-axis with a lower toroidal energy flows. The breakthrough of separatrix line physical features observed in CAM drive experimental test data are part of the NSF Phase I discoveries.

Evidence points to external angular momentum force couples being along the torus tube tangent slot opening. With working fluid external force couple transfer, the angular velocity vector polhode moves from X-MOI (high energy) to Z-MOI (lower energy) following the separatrix line towards the Y-axis and to Z-axis lower energy polhode. The angular velocity $\boldsymbol{\omega}$ movement is distinct in the direction for CW and CCW working fluid circulation. From Poinsot's geometric solution, this represents a physical mechanisms that transfers momentum or energy in rotational motion. HTV Phase I data analysis supports this physical interpretation for Figs. 6 and 9. Linear regression analysis of measured force and differential EDF power shows a negative slope for CW working fluid and a positive slope for CCW working fluid. These results are expected when the poloidal flow along X-axis is below the separatrix line for CW working fluid.

The CCW linear regression positive slope result, Fig. 9, is consistent with the poloidal vortex torus tube location and on Poinsot's geometric ellipsoid, Fig. 8. The linear result demonstrates the physical interface between working fluid angular momentum and rotational energy from the physical CAM interpretation. The slope of linear regression data analysis is an important Phase I demonstrable result.

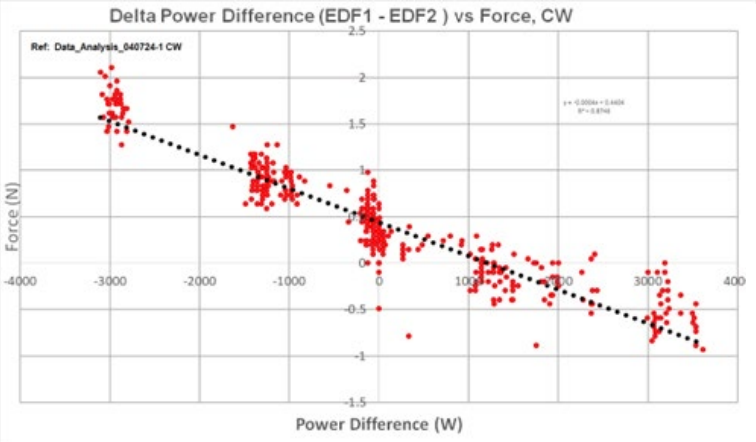

Figure 6: CW Working Fluid Linear Regression with Negative Slope

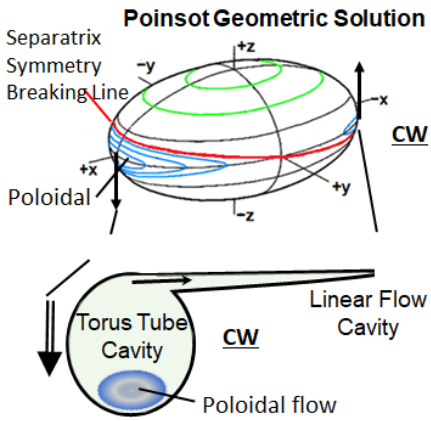

Figure 7: CW Symmetry Breaking Produces Force Couples Consistent with Poinsot Solution

For the poloidal flow above the separatrix line, Fig 8, the slope is positive with CCW working fluid. It is the X-axis poloidal flow position with respect to the separatrix line that determines the angular momentum force couple directions. This poloidal flow position is consistent for both CW and CCW working fluid flow. A cross-sectional orientation of the torus tube poloidal flow is shown with respect to the linear flow cavity, Figs. 7 and 8.

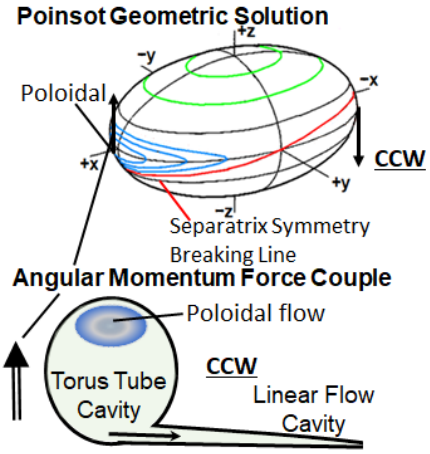

Figure 8: CCW Symmetry Breaking Produces Force Couples with Poinsot

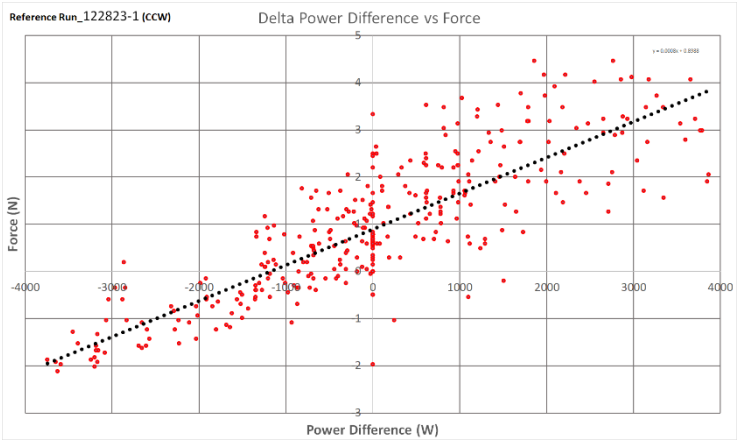

Figure 9: CCW Working Fluid Linear Regression with Positive Slope

A summary, Table 2, highlights Poinsot's rotational dynamics, CAM drive, and the physical effects on CAM drive working fluid structures.

Table 2: Summary of Rotational Fluid Dynamics and CAM Drive

Topics	CAM Drive	Working Fluid Rotation
Poinsot Ellipsoid Dynamics	Correlates CAM principles with CAM drive experiments for simultaneous working fluid angular velocity about X-MOI and Z-MOI	Polhode and herpolhode map **ω** between X-MOI (poloidal) and Z-MOI (toroidal)
NSF Phase I Data Analysis	Linear regression slopes: negative for CW and positive for CCW flows	Poloidal flow position relative to separatrix line determines force couple direction
Tangency Condition	Angular velocity **ω** is on both inertia ellipsoid and invariable plane, **H**=const.	Herpolhode in linear flow cavity is tangential in adherence to CAM constraints

4. Linear Working Fluid Flow Data Analysis

CAM drive linear flow structure provides a novel conversion of working fluid into a linear flow through a tangential torus slot. This diffuser process mimics a rocket thruster nozzle with increases in propulsive efficiency and momentum transfer, for example, a larger radial linear flow structure produces higher efficiency. Under nominal CAM drive conditions, about 35% to 40% of the torus tube mass flow rate from the EDFs moves into the linear flow cavity as a tangent flow. In Fig. 10, even though all the EDF working fluid is initiated along that X-axis, inside the linear cavity the flow is not defined along this axis. Future Minimum Viable Product (MVP) linear flow designs removed this section, since it provided no useful purpose. Most importantly, the working fluid flow along the torus tube tangent slot opening was never impeded.

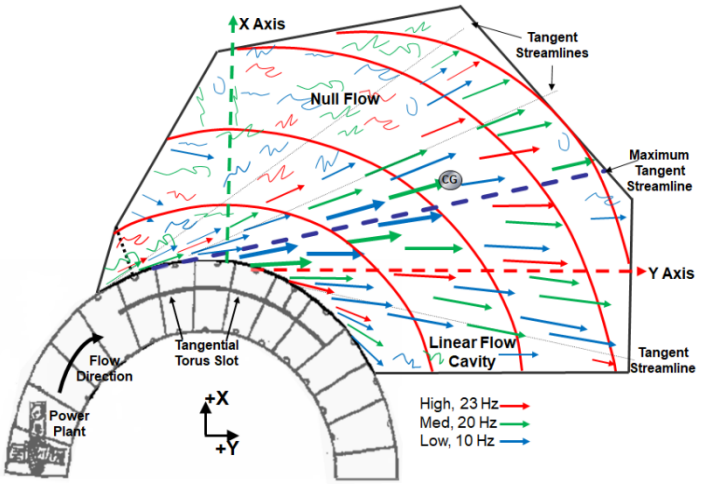

Figure 10: Linear Flow Cavity Flow Structure

Tangential working fluid flow is similar to projectile objects leaving a shepherd's sling. Experimental measurements used pitot tubes for working fluid 'projectile' velocity. Pitot tubes are fluid flow total and static pressure energy sensors based on Bernoulli's principle, $P_{total}=P_{static}+P_{dynamic}$. The dynamic pressure, $\frac{1}{2}\rho V^2$, is measured on pressure gauges by subtracting the total from static pressure. This slotted flow transfer results in a uniform flow field inside the linear flow structure along tangent lines, Fig. 10. The linear flow is driven by CAM and tangency condition. To meet CAM constraints, the angular velocity **ω** must lie both on the inertial ellipsoid and the invariable plane perpendicular for a constant angular momentum, **H**. The tangency condition couples the working fluid inside the torus tube geometry, as an inertia ellipsoid, to its motion in inertial space (invariable plane). The tangent condition ensures the working fluid on the invariable plane will enter the linear flow cavity as a tangential flow, which defines the herpolhode motion.

At the torus tube interface, working fluid rotational energy is converted directly to linear kinetic energy (K_e), with $T_{rot}=\frac{1}{2}I\omega^2$, $I=MR^2$, and $\omega=V/R$, which yields $T_{rot}=\frac{1}{2}MR^2(V/R)^2=\frac{1}{2}MV^2$. At the torus tube interface, M represents the working fluid mass, and rotational energy T_{rot} is equivalent to linear kinetic energy, $K_e=\frac{1}{2}MV^2$ that exits the torus tube. Kinetic energy is a function of velocity squared, $f(V^2)$ and causes a large potential flow inside the linear flow cavity. This physical condition is called the 'David and Goliath' effect that can take down giants in a truly biblical context.

5. Analysis of NSF Phase I Measured Force Data

The CAM hypothesis with a single torus tube is verified in NSF Phase I. The CW and CCW polarity and separate forces for EDF1 and EDF2 are measured by power throttle control for both electrical motors from 1kW to 3kW. Fig. 11 shows actual CW working fluid results shown with a red line being the difference between EDF1 and EDF2 power. The black line is the measured force data.

During the NSF Phase I, experiments used two EDFs, each with maximum air flow rate of 0.86 kg/sec, and force measurements were made on a hinged counter-balanced fulcrum with a weight scale device. For data comparison, simultaneous data was recorded from weight scale and EDF motor electrical power.

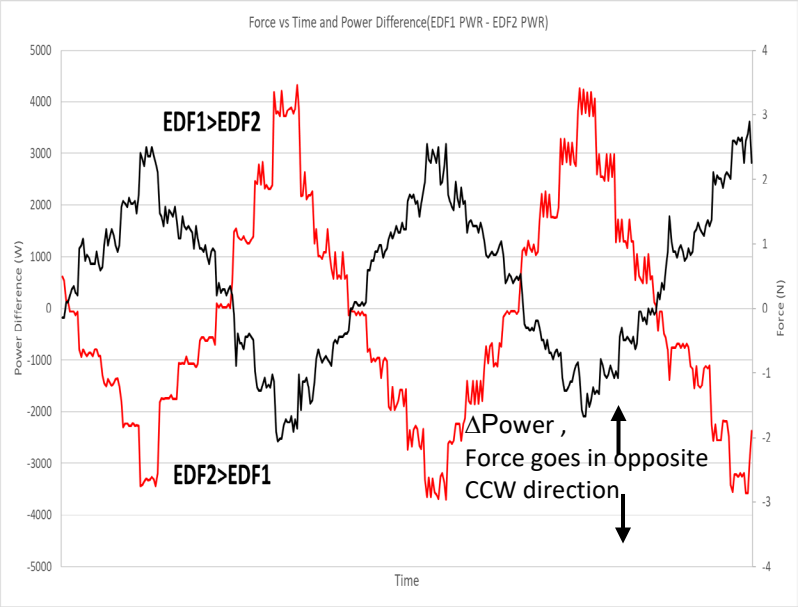

Figure 11: Clockwise (CW) Working Fluid

For Figs. 11 and 12, when EDF1 power is greater than EDF2, then the red line power difference is on the top of the graph. The opposite EDF1 and EDF2 power condition is on the bottom of the graph, where EDF2 power is greater than EDF1. The observed and measured forces are different for working fluid CW and CCW polarity direction, as the force direction is inverted. When working fluid is moving in CW direction, Fig. 11, then the force is coupling with EDF1 power associated with negative (retro) force and EDF2 power with positive (react) force. The measured resultant force tracks all the EDF input power, which is controlled by the operator.

When working fluid is moving in the CCW direction, Fig. 12, then the force is coupling with EDF1 power associated with positive (react) force and EDF2 power with negative (retro) force. This fundamental feature of CAM drive is identified as a Phase I discovery. In Section 3, the CAM analysis suggests measured and inverted force are the result of the change in separatrix line slope with respect to the CW and CCW working fluid flow direction. The physical meaning is the negative CW slope separatrix line causes an inversion for the force and differential power, Fig. 11. While the positive CCW slope separatrix results in the force tracking the differential power, Fig. 12. This explanation allows for consistency between Poinsot's geometric interpretation and measured force results. Data analysis results and measurement are repeatable across multiple NSF Phase I HTV test cases, where all test data results are similar to Figs. 11 and 12.

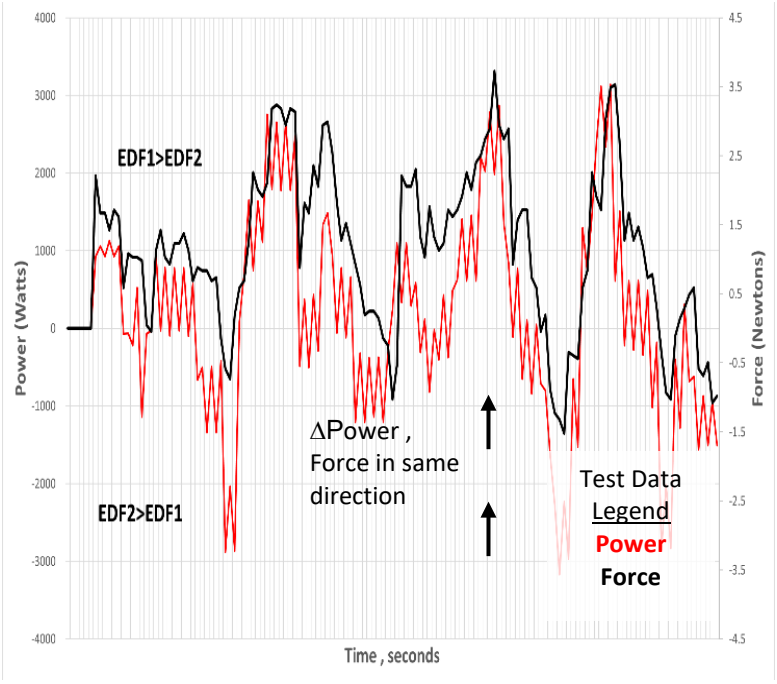

Figure 12: Counterclockwise (CCW) Working Fluid

The Phase I force and power test data analysis provided an assessment into the average and peak performance for CW and CCW working fluid circulation, Fig. 13. Data sufficiency was used for average and peak analysis with over 8100 test data points to assess the performance. CCW working fluid is identified as EDF1 and EDF2. The CW working fluid is identified as EDF3 and EDF4. The red bars for EDF2 and EDF4 are retro operations and the blue bars for EDF1 and EDF3 are reactive operations. With adding CAM drive throttle control for increased commercialization performance, the of LEO, medium (MEO), and geosynchronous (GEO) Earth Orbit transfer operations are looking good.

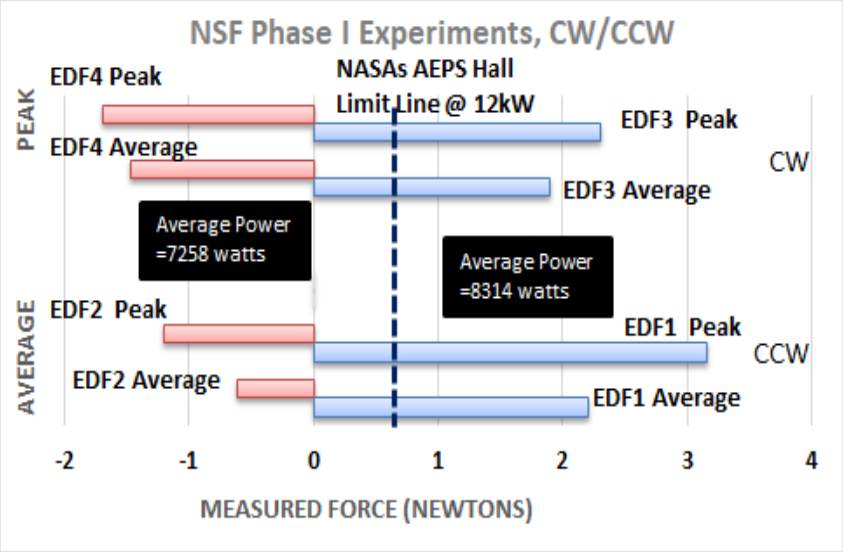

Figure 13: NSF Phase I Average and Peak Performance

The Fig. 13 bar graph thruster performance is compared with NASA's Advanced Electric Propulsion System (AEPS) Hall effects thruster, which shows the stark reality of CAM drive future of orbital transfer systems. The AEPS performance of 0.59N at 12.5kW is lower than the sum of EDF1 and EDF3 average measured thrust of 4N at 8.3kW with peak performance over 5N of thrust. The added value of CAM drive propellantless performance includes $6,500/kg launch cost saving for fuel, 3-months extra operational time saved with faster GEO telecom satellite transit and mission extension, resulting in $110M mission revenue.

6. Minimum Viable Product (MVP) Performance

Discoveries and advancements from the NSF Phase I concept demonstration were used for MVP small satellite (smallsat) commercialization for LEO and Very-LEO (VLEO) operations. In order to provide propellantless propulsion with reduced power for the smallsat market, VSS developed a proposal to Montgomery County Technology Innovation Fund for commercializing a low power MVP. The VLEO offers significant advantages of sustained operations at 200 to 400km altitude. The measured MVP test performance is shown in Fig. 14. By comparing thrust and power performance in Fig. 13 and 14, the MVP is a vast improvement from NSF Phase I concept demonstration.

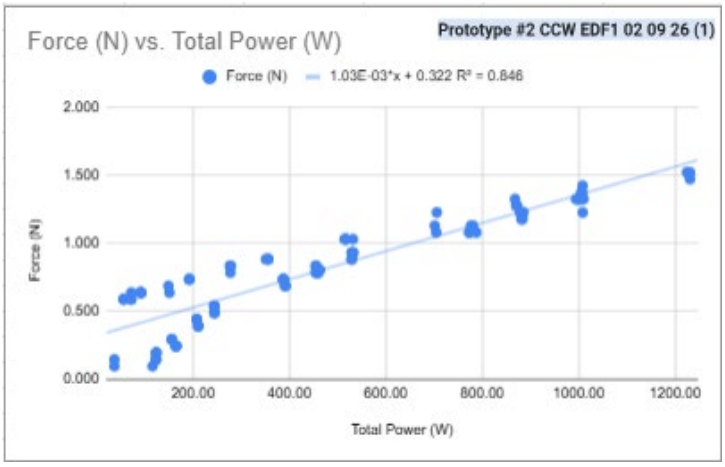

Figure 14: MVP Predicted Performance with Low Power

Compared to higher traditional earth orbits, the VLEO smallsats contend with intense atmospheric drag, which accelerates orbital decay and demands near-constant propulsion adjustments to stay in an operational orbit. MVP provides efficient propellantless propulsion for VLEO smallsats to extend system lifespans and operator revenue. For example, a smallsat operating below 200km must orbit raise within a week to 10-day or plan for re-entry into the earth's atmosphere.

Montgomery County Tech Fund was very successful in developing 3 different MVP prototypes and quickly moving the MVP CAM drives to testing. This accomplishment was achieved by using digital design CAD modeling and 3D additive fabrication, which facilitated multiple prototype interface fit checks. The MVP approach used modular designs with the only differences being prototypes linear flow structures and electric ducted fan inlet diameters of 7cm and 12cm. These difference allowed test characterization of prototype performance and optimal protoflight design for qualification testing.

Another MVP success story is the linear flow structure test and design analysis. From preliminary test data, a larger prototype #2 linear flow structure doubled the propulsive efficiency, more thrust force and less power, over smaller prototype #1 structure. Advancing protoflight design involves engineering structural analyses improvements to validate proper loads, which are verified during qualification testing. The structure modes are the driving operating condition, which needs greater design rib thickness and added fin support, Fig. 15. The modal analysis showed 1st and 2nd structural modes at 150Hz and, which avoids resonance with the working fluid circulation rate at 70Hz.

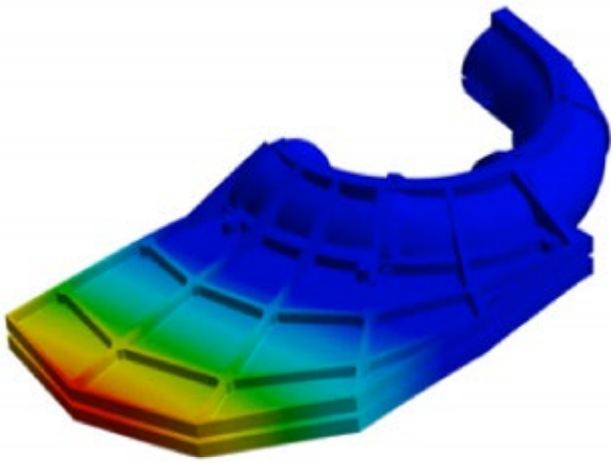

Figure 15: Protoflight #2 Structure Design Analysis

7. Helmholtz Vortex Theorems and Inertial Frame Dragging

An important aspect of NSF Phase I STTR funding is the broader impacts and intellectual merit objectives from CAM drive propellantless thrust technology. There is significant and meaningful value in further developing the CAM drive technology from NSF Phase I discoveries. One example is associating Helmholtz vortex theorems with CAM principles. As with all rotating systems in nature, Helmholtz vortex theorems must satisfy conservation of angular momentum. This is accomplished with a minor modification by using area per unit mass to assess vortex strength.

The derivation of Herman Von Helmholtz hydrodynamic vortex motion equations are valid for ideal, inviscid fluids. Although, these equations are summarized as theorems, the formulation can provide insights into real flows with specialized viscous effects, such as boundary layer and poloidal flows, Table 3. Helmholtz 1st vortex theorem expresses conservation, where vortex tube, circular cross-sectional area 'A' and angular velocity **ω**, aligns with CAM circulation. Helmholtz analysis determined that the product of vortex cross-section area and angular velocity are constant along the vortex streamline. The 1st theorem for vortex flows have similarities to Poinsot's geometric constructions, where angular momentum **H**=I·**ω** = constant, for rigid body rotation, where MOI is a function of cross-section area.

Table 3: Helmholtz Three Vortex Theorems

Theorem	Statement	Applications and Conditions
1. Conservation of Vortex Strength	Fluid circulation around a vortex tube remains constant along its length over time.	Vortex tube cross-sectional area *A* and angular velocity **ω** satisfy ω x A=constant (poloidal vortex stretching) and CAM.
2. Conservation of Vortex Lines	Vortex lines move with fluid particles, resulting in continuous fluid element forming a vortex line, surfaces, and tubes that remain coherent fluid flow structures.	Vorticity and vortex flows are frozen into the flow in inviscid fluids, and fluid flow elements initially on a vortex line remain on it indefinitely. Extending this theorem to an inertial frame, the frame is dragged along the vortex line for coherent fluid flow structures.

3. Irrotational Flow Persistence	Fluid elements initially free of vorticity remain irrotational, zero vorticity condition.	Vorticity cannot spontaneously generate in ideal fluids. Zero vorticity is established by counter-rotating vortex structures.

Helmholtz 1st theorem is the subject of Montgomery County Technology Innovation Fund MVP design development, engineering study, and testing. In Fig. 4, the 7cm diameter torus tube yields a cross-section area (A) of 38.5cm^2. The EDF inlet area has a diameter of 12cm for a cross-section area of 113.1cm^2. This gives an increase working fluid circulation factor of 3 times, which yields predicted thrust performance estimate of 3.6N at 1kwatt of electrical power, Table 1.

For an inviscid and incompressible flow, Helmholtz 2nd vortex theorem assessed that a fluid particle must move along the streamline within the vortex flow. The 2nd vortex theorem is applied once the inertial frame of a vortex is set in motion, i.e., Helmholtz 3rd vortex theorem, the initial fluid flow properties must travel with the vortex. VSS measured and verified this phenomenon during pre-NSF Phase I testing, where working fluid strength directly correlated with vortex circulation flow at different EDF power settings. These measurements reinforced the inertial working fluid properties within the vortex flow field.

In this way, once the vortex is set in inertial motion, the inertial pointing attitude is fixed and is dragged along the vortex streamline within the working fluid physical properties. When the X-axis angular momentum vector is initiated at the EDF, the angular momentum vector is established in inertial space. From Helmholtz 2nd vortex theorem, the working fluid angular momentum and element frame is moved or dragged along the streamlines within the vortex flow. Helmholtz hydrodynamic vortex equations identified inertial frame dragging 30 years before Einstein's general relativity, which established frame dragging as a theoretical physical property.

8. Intellectual Property and Future Research Discoveries

The CAM Drive technology innovation began with an invention. In March 2020, US Patent and Trademarks Office granted a patent, #10,604,255, which describes the preliminary design concept, single smart manufacturing product language, and work breakdown structure for controlling CAM drive fabrication and assembly. Research discoveries prior to Phase I are identified in Table 4.

Table 4: CAM drive Patented Discoveries (Pre-NSF Phase I)

Discovery	Patented	Experimental Observations
CAM drive force is function of EDF power	Yes	Force is measurable and repeatable
CAM Drive™ defines basic machine	Yes	Fluid flow energy transfer between minimum and maximum
Linear fluid flow	Yes	Flow is perpendicular and tangent to EDF max energy input
Poloidal flow field	Yes	Represents maximum energy in flow with CAM
Linear, poloidal, and toroidal flow fields	Yes	Fluid structures fixed in position with CAM
Force from rotational motion of fluid	Yes	Analysis conserves system angular momentum
Double Tori Design	Yes	Double tori (2-CAM drives) design for CW/CCW operations and to increase system reliability

In NSF Phase I, an additional discovery was made regarding CW and CCW reaction forces and angular momentum couple polarity. Per the Bayh-Dole Act (35 USC 200-204) and federal regulations (37 CFR Part 401), NSF Phase I angular momentum couple discoveries were registered on NIST iEdison database with # 455437022. A utility patent application, #19/361,094, pending, has been filed at USPTO. Future research topic areas include modelling a rotating system of particles with minimum and maximum fluid flow energy transfer and torque free motion; deeper investigation into irrotational flow condition in Helmholtz #3 Vortex Theorems and CAM inertial coordinate frame dragging; refine CAM field equations for rotating fluid flows; and define entropy cycling in rotating fluid flows.

9. Summary

NSF Phase I showed that CAM drive operates at a level much deeper than a conserved change in angular momentum, $\Delta\mathbf{H}=0$. CAM is more than symmetric spinning gyroscopic top or the competitive ice skater

performing a graceful triple lutz while flying through the air. A broader CAM assessment allows planetary scientists and astrophysicist to analyze celestial objects with respect to the angular velocity or inertial mass distribution. For all rotating phenomenon in nature, angular momentum is conserved.

Ignoring the proper application of CAM in analyses results in errors and a significant lack of understanding in the physics of rotating systems. Natural invariant properties resulting in asymmetric system separatrix lines allows CAM drive to satisfy conservation of angular momentum with measurable forces from Euler's moment equations and Poinsot's solution. NSF STTR Phase I demonstrated the propulsive performance advantage of conservation of angular momentum. For the future of propellantless CAM drive, the Montgomery County Technology Innovation Fund with MVP designs can increase the beneficial economics of space commerce.

References

[1] Millis, Marc G., "Assessing Potential Prop Breakthroughs," NASA TM-2005-213998, Dec. 2005, pp. 17-18.
[2] Kalpakli, Athanasia, "Experimental study of turbulent flows through pipe bends," Royal Institute of Technology SE–100, April 2012, Section 2 and Figure 2.2.
[3] Homicz, Gregory F, "Computational Fluid Dynamics Simulations of Pipe Elbow Flow," Sandia National Laboratories, SAND2004–3467, 2004, Figure 5.
[4] Likins, Peter W., "Effects of Energy Dissipation on the Free Body Motions of Spacecraft," JPL Technical Report No. 32-860, July 1966, Appendices A and C.